Springer

Journal of
Mechanical
Science and
Technology

Journal of Mechanical Science and Technology 22 (2008) 1269~1278

www.springerlink.com/content/1738-494x

A unified brittle fracture criterion for structures with sharp V-notches under mixed mode loading

Jin Kwang Kim and Sang Bong Cho*

Division of Mechanical Engineering and Automation, Kyungnam University, Masan 631-701, Korea

(Manuscript Received December 31, 2007; Revised February 17, 2008; Accepted March 23, 2008)

Abstract

A unified brittle fracture criterion for cracks and V-notches under mixed mode loading is proposed by extending the maximum circumferential stress criterion and Novozhilov's criterion. The mixed mode fracture toughness and crack orientation of PMMA plates with a sharp V-notch are predicted by the proposed criterion. Tests were also carried out in order to investigate the mixed mode fracture of the PMMA plates. The fracture criterion is validated by comparison to experimental results.

Keywords: Sharp V-notch; Maximum circumferential stress criterion; Unified brittle fracture criterion; Stress intensity factor; RWCIM

1. Introduction

The stress fields around the tips of cracks or sharp V-notches, as shown in Fig. 1, are generally singular. As a result, crack initiation occurs at these sharp corners. The efforts of many engineering investigators have been focused on developing a unified method to evaluate the fracture strength of cracks and sharp V-notches. Therefore, an interesting problem in fracture mechanics is to establish a simple and accurate fracture criterion that enables the prediction of crack initiation and crack orientation near the tip of sharp V-notches under mixed mode loading.

Several fracture criteria to evaluate the fracture toughness and fracture angle, such as the maximum circumferential stress criterion [1], the minimum strain energy density criterion [2], and the maximum energy release rate criterion [3], have been proposed. The maximum circumferential stress criterion is simple and the most commonly used. This criterion states the following: (1) A crack propagates from the V-notch crack tip along the direction θ_o for which the circumferential stress is maximum, and (2) a fracture occurs when the maximum circumferential stress $\sigma_{\theta\theta}$ reaches a critical stress value σ_c, which is equal to the fracture stress under the uniaxial tension.

Seweryn [4] proposed a fracture criterion for sharp V-notches in brittle materials under Mode I loading; it is based on Novozhilov's criterion and the maximum circumferential stress criterion. Novozhilov's proposal [5] states that a fracture may occur when the mean stress along a small distance ahead of the tip of

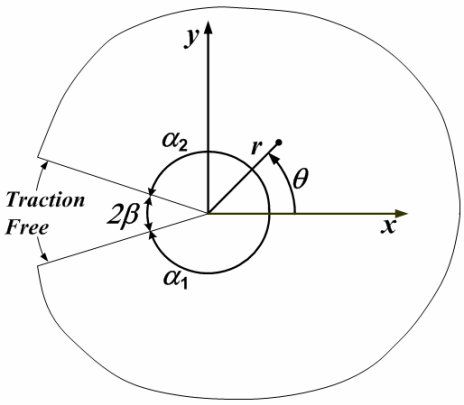

Fig. 1. Configuration of a V-notch with traction-free faces.

*Corresponding author. Tel.: +82 55 249 2620, Fax.: +82 55 249 2617
E-mail address: sbcho@kyungnam.ac.kr
DOI 10.1007/s12206-008-0315-y

a V-notch reaches the critical breaking stress. Several researchers [6-11] have also presented theoretical and experimental results for V-notch problems. In their studies, the results for either Mode I or Mode II are presented, but there are not many results for mixed mode loading. Seweryn et al. [12] studied the mixed mode loading problems. The criterion was formulated by combining the normal stress in perpendicular direction and the shear stress in parallel direction to crack propagation. Grenestedt et al. [13] carried out a similar research on cracks and V-notches in an expanded polyvinyl chloride (PVC) form. Hallstrőm and Grenestedt [14] also studied mixed mode problems of cracks and V-notches. As they indicated in their works, the fracture direction θ_o varies with the distance r for all V-notches except cracks under the mixed mode loading. Due to this feature, it is difficult to apply the maximum circumferential stress criterion and Novozhilov's criterion to mixed mode problems.

In this paper, the following extensions to the maximum circumferential stress criterion and Novozhilov's criterion are assumed: (1) A crack propagates along θ_o for which the circumferential stress is maximum at a distance of $r = d_o$ from the V-notch or the crack tip, and (2) a fracture occurs when the mean circumferential stress $\bar{\sigma}$ reaches the critical stress σ_c, which is equal to the fracture stress in uniaxial tension.

The extended maximum circumferential stress criterion and Novozhilov's criterion are applied to predict the fracture toughness and crack orientation for V-notches under a mixed load. The effectiveness and validation of the proposed criterion are discussed by comparison of the experimental results of polymethyl methacrylate (PMMA) material with the predicted results. In order to determine the critical stress intensity factors from the fracture loads obtained by the fracture test of a PMMA plate with arbitrary wedge angles under mixed mode loading, the reciprocal work contour integral method (RWCIM) [15-18] based on Betti's reciprocal work theorem and finite element analysis is used. The formulation of the RWCIM is given in Ref. [19]. The verification of the RWCIM will be discussed for the mixed mode condition.

2. Stress and displacement fields around the tip of a sharp V-notch

We analyze a sharp V-notch in a linear two-dimensional elastic body, as shown in Fig. 1. The boundary condition for both the notch surfaces with arbitrary wedge angles $\theta = -\alpha_1$ and α_2 is traction-free. In this study, the wedge angles are considered to be equal, that is, $\alpha_1 = \alpha_2 = \alpha$. In Williams' eigenfunction expansion series [20], it is well known that the eigenvalues of Mode I can be obtained from $\lambda \sin(2\alpha) + \sin(2\alpha\lambda) = 0$ and those of Mode II can be calculated from $-\lambda \sin(2\alpha) + \cos(2\alpha\lambda) = 0$. Subsequently, the eigenvalues of the opening and sliding mode are denoted as φ and η, respectively. The stress and displacement fields for structures with a sharp notch are described in terms of polar coordinates (r, θ) centered at the tip of a V-notch as follows [18]:

$$u_j(r,\theta) = \sum_{n=1}\left[\frac{r^{\varphi_n} A_{Rn}}{2\mu} g_{jn}^{I}(\theta) + \frac{r^{\eta_n}(-A_{In})}{2\mu} g_{jn}^{II}(\theta)\right], \quad (j = r,\theta) \tag{1}$$

$$\sigma_{ij}(r,\theta) = \sum_{n=1}\left[\frac{A_{Rn}}{r^{1-\varphi_n}} f_{ijn}^{I}(\theta) + \frac{(-A_{In})}{r^{1-\eta_n}} f_{ijn}^{II}(\theta)\right], \quad (i,j = r,\theta) \tag{2}$$

where

$$\begin{Bmatrix} g_{rn}^{I}(\theta) \\ g_{\theta n}^{I}(\theta) \end{Bmatrix} = \begin{Bmatrix} (\kappa - \varphi_n)C[(\varphi_n - 1)\theta] + C[(\varphi_n + 1)\theta - \\ (\kappa + \varphi_n)S[(\varphi_n - 1)\theta] + S[-(\varphi_n + 1)\theta + \end{Bmatrix}, \begin{matrix} 2\varphi_n\alpha] + \varphi_n C[-(\varphi_n + 1)\theta + 2\alpha] \\ 2\varphi_n\alpha] + \varphi_n S[-(\varphi_n + 1)\theta + 2\alpha] \end{matrix}\Bigg\}$$

$$\begin{Bmatrix} g_{rn}^{II}(\theta) \\ g_{\theta n}^{II}(\theta) \end{Bmatrix} = \begin{Bmatrix} (\kappa - \eta_n)S[(\eta_n - 1)\theta] - S[(\eta_n + 1)\theta - \\ -(\kappa + \eta_n)C[(\eta_n - 1)\theta] - C[(\eta_n + 1)\theta - \end{Bmatrix}, \begin{matrix} 2\eta_n\alpha] - \eta_n S[-(\eta_n + 1)\theta + 2\alpha] \\ 2\eta_n\alpha] + \eta_n C[-(\eta_n + 1)\theta + 2\alpha] \end{matrix}\Bigg\}$$

$$\begin{Bmatrix} f_{rrn}^{I}(\theta) \\ f_{\theta\theta n}^{I}(\theta) \\ f_{r\theta n}^{I}(\theta) \end{Bmatrix} = \begin{Bmatrix} \varphi_n\{(3 - \varphi_n)C[(\varphi_n - 1)\theta] + C[(\varphi_n + 1)\theta - \\ \varphi_n\{(\varphi_n + 1)C[(\varphi_n - 1)\theta] - C[(\varphi_n + 1)\theta - \\ \varphi_n\{(\varphi_n - 1)S[(\varphi_n - 1)\theta] + S[-(\varphi_n + 1)\theta + \end{Bmatrix}, \begin{matrix} 2\varphi_n\alpha] + \varphi_n C[-(\varphi_n + 1)\theta + 2\alpha]\} \\ 2\varphi_n\alpha] - \varphi_n C[-(\varphi_n + 1)\theta + 2\alpha]\} \\ 2\varphi_n\alpha] + \varphi_n S[-(\varphi_n + 1)\theta + 2\alpha]\} \end{matrix}\Bigg\}$$

and

$$\begin{Bmatrix} f_{rrn}^{II}(\theta) \\ f_{\theta\theta n}^{II}(\theta) \\ f_{r\theta n}^{II}(\theta) \end{Bmatrix} = \begin{Bmatrix} \eta_n\{(3 - \eta_n)S[(\eta_n - 1)\theta] - S[(\eta_n + 1)\theta - \\ \eta_n\{(\eta_n + 1)S[(\eta_n - 1)\theta] + S[(\eta_n + 1)\theta - \\ -\eta_n\{(\eta_n - 1)C[(\eta_n - 1)\theta] + C[-(\eta_n + 1)\theta + \end{Bmatrix}, \begin{matrix} 2\eta_n\alpha] - \eta_n S[-(\eta_n + 1)\theta + 2\alpha] \\ 2\eta_n\alpha] + \eta_n S[-(\eta_n + 1)\theta + 2\alpha] \\ 2\eta_n\alpha] - \eta_n C[-(\eta_n + 1)\theta + 2\alpha] \end{matrix}\Bigg\}$$

Here, $\kappa = (3-4\nu)$ for a plane strain and $\kappa = (3-4\nu)/(1+\nu)$ for a plane stress, C = cosine, and S = sine. μ and ν are the shear modulus and Poisson's ratio, respectively. A_{Rn} and A_{In} are undetermined eigenvector coefficients. The variation of the singular eigenvalues with respect to the wedge angle is shown in Fig. 2. In this research, the Mode I stress intensity factor K_I^n, which is related to the singular Mode I eigenvalue φ_1 and the undetermined eigenvector coefficient $A_{R1}(\varphi_1)$, is defined by the following Eq. (5). Moreover, the Mode II stress intensity factor K_{II}^n can be described by using η_1 and $A_{I1}(\eta_1)$, as shown in Eq. (6). η_1 is the singular eigenvalue of the sliding mode and $A_{I1}(\eta_1)$ is the undetermined eigenvector coefficient associated with η_1. By using only two singular terms with φ_1 and η_1 in the eigenfunction expansion series, the stress and displacement fields around the V-notch tip can be represented as follows:

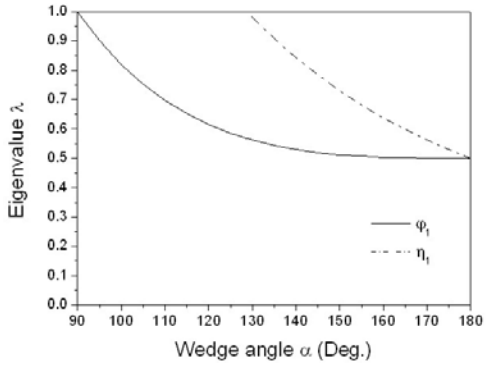

Fig. 2. Variation of eigenvalues with the wedge angle α.

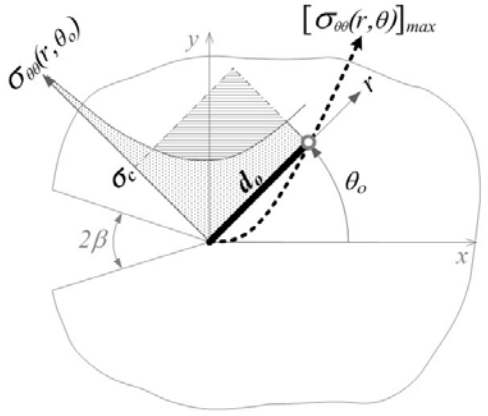

Fig. 3. The mean circumferential stress over the length d_o near the tip of a V-notch.

$$u_j(r,\theta) = \frac{r^{\varphi_1}}{2\mu}\frac{K_I^n}{\sqrt{2\pi}}g_{j1}^I(\theta) + \frac{r^{\eta_1}}{2\mu}\frac{K_{II}^n}{\sqrt{2\pi}}g_{j1}^{II}(\theta), \quad (j=r,\theta) \tag{3}$$

$$\sigma_{ij}(r,\theta) = \frac{K_I^n}{\sqrt{2\pi}\,r^{1-\varphi_1}}f_{ij1}^I(\theta) + \frac{K_{II}^n}{\sqrt{2\pi}\,r^{1-\eta_1}}f_{ij1}^{II}(\theta), \quad (i,j=r,\theta) \tag{4}$$

where

$$K_I^n = \lim_{r\to 0}\left[\sqrt{2\pi}\,r^{1-\varphi_1}\,\frac{\sigma_{\theta\theta}}{f_{\theta\theta1}^I(0)}\right] = \sqrt{2\pi}A_{R1}, \tag{5}$$

$$K_{II}^n = \lim_{r\to 0}\left[\sqrt{2\pi}\,r^{1-\eta_1}\,\frac{\sigma_{r\theta}}{f_{r\theta1}^{II}(0)}\right] = -\sqrt{2\pi}A_{I1}. \tag{6}$$

3. Brittle fracture criterion for V-notches under mixed mode loading

As stated in introduction, the direction of the maximum circumferential stress varies with the distance r for all V-notches except cracks under mixed mode loading. For this reason, it is difficult to apply the maximum circumferential stress criterion and Novozhilov's criterion to mixed mode problems.

The following extensions to the maximum circumferential stress criterion and Novozhilov's criterion are assumed: (1) A crack propagates along the direction θ_o for which the circumferential stress is maximum at a small distance $r = d_o$ from the V-notch or crack tip and (2) a fracture occurs when the value of $\bar{\sigma}$ reaches that of σ_c, which is equal to the fracture stress in uniaxial tension.

$\bar{\sigma}$ can be expressed as follows:

$$\bar{\sigma} = \frac{1}{d_o}\int_0^{d_o}\left[\sigma_{\theta\theta}(r,\theta_o)\right]dr, \tag{7}$$

where d_o is assumed to be a material constant and the crack orientation θ_o is the angle producing $[\sigma_{\theta\theta}(d_o,\theta)]_{\max}$ on the circumference of radius, $r = d_o$ as shown in Fig. 3.

By substituting the circumferential stress component $\sigma_{\theta\theta}$ of Eq. (4) into Eq. (7), the following expression is obtained:

$$\bar{\sigma} = \frac{1}{\sqrt{2\pi}}\left[\frac{1}{\varphi_1\ d_o^{1-\varphi_1}}K_I^n f_{\theta\theta1}^I(\theta_o) + \frac{1}{\eta_1\ d_o^{1-\eta_1}}K_{II}^n f_{\theta\theta1}^{II}(\theta_o)\right]. \tag{8}$$

$\bar{\sigma}$ is related to the breaking tensile stress σ_c which can be obtained from the tensile test of an un-notched specimen:

$$\bar{\sigma} \geq \sigma_c . \tag{9}$$

The brittle fracture of an engineering structure will occur when the value of $\bar{\sigma}$ reaches that of σ_c. The following fracture criterion is obtained by Eqs. (8) and (9):

$$\frac{1}{\sqrt{2\pi}}\left[\frac{1}{\varphi_1 \; d_o^{1-\varphi_1}}\left(\frac{K_{Icr}^n}{\sigma_c}\right) f_{\theta\theta 1}^I(\theta_o) + \frac{1}{\eta_1 \; d_o^{1-\eta_1}}\left(\frac{K_{IIcr}^n}{\sigma_c}\right) f_{\theta\theta 1}^{II}(\theta_o)\right] = 1 , \tag{10}$$

where K_{Icr}^n and K_{IIcr}^n are the critical values of K_I^n and K_{II}^n under the mixed mode loading condition, respectively.

Since K_{II}^n becomes zero in the case of Mode I, Eq. (10) can be represented as follows:

$$d_o = \left[\frac{1}{\sqrt{2\pi}}\left(\frac{f_{\theta\theta 1}^I(0)}{\varphi_1}\frac{K_{Icr}^n}{\sigma_c}\right)\right]^{1/(1-\varphi_1)} . \tag{11}$$

In the case of crack problems, the singular eigenvalue for Mode I is obtained as $\varphi_1 = 0.5$ and K_I^n is denoted as K_I for easy identification. A fracture occurs when the value of K_I reaches that of the fracture toughness K_C. Therefore, d_o can be obtained from K_C and σ_c by employing experimental results [4]:

$$d_o = \frac{1}{2\pi}\left(\frac{2K_C}{\sigma_c}\right)^2 . \tag{12}$$

As stated above, θ_o can be determined by using the condition of $\partial\sigma_{\theta\theta}(r,\theta)/\partial\theta = 0$ at $r = d_o$ from Eq. (13).

$$(\sigma_{\theta\theta})' = \frac{K_{Icr}^n}{\sqrt{2\pi} \; d_o^{1-\varphi_1}}(f_{\theta\theta 1}^I(\theta))' + \frac{K_{IIcr}^n}{\sqrt{2\pi} \; d_o^{1-\eta_1}}(f_{\theta\theta 1}^{II}(\theta))' = 0 , \tag{13}$$

where the prime symbol represents differentiation. From Eqs. (10) and (13), the critical values of K_I^n and K_{II}^n for the mixed mode condition can be obtained as follows:

$$K_{Icr}^n = \frac{\sqrt{2\pi} \; d_o^{1-\varphi_1}}{\frac{1}{\varphi_1} f_{\theta\theta 1}^I(\theta_o) - \frac{1}{\eta_1} f_{\theta\theta}^{II}(\theta_o)\left[\frac{(f_{\theta\theta 1}^I(\theta))'}{(f_{\theta\theta}^{II}(\theta))'}\right]_{\theta=\theta_o}} \sigma_c , \tag{14}$$

$$K_{IIcr}^n = \frac{\sqrt{2\pi} \; d_o^{1-\eta_1}}{\frac{1}{\eta_1} f_{\theta\theta 1}^{II}(\theta_o) - \frac{1}{\varphi_1} f_{\theta\theta 1}^I(\theta_o)\left[\frac{(f_{\theta\theta 1}^{II}(\theta))'}{(f_{\theta\theta 1}^I(\theta))'}\right]_{\theta=\theta_o}} \sigma_c . \tag{15}$$

A unified brittle fracture criterion for cracks and V-notches under mixed mode loading was obtained by extending the maximum circumferential stress criterion and Novozhilov's criterion. The mixed mode fracture toughness and crack orientation of PMMA plates with a sharp V-notch can be predicted by this criterion.

4. Experiments and discussions

4.1 Specimens and the loading fixture

Tests were carried out to measure the critical loads at fracture and the fracture angles of plates with a sharp V-notch. The photograph and configuration of the loading fixture with a specimen are shown in Fig. 4. The loading fixture is of Richard's type [21], and it can be used for various mixed loading modes by changing the loading angle γ. The specimen material for the LEFM test is PMMA, which is brittle. The specimen dimensions are as follows: height H = 60 mm, width W = 40mm, notch length a = 20mm and thickness t = 5mm. The notches in the specimens were shaped by a vertical milling machine and were constrained by two steel plates with a notch angle of 2β = 150º. The total number of specimens prepared was 90: 18 specimens for each notch angle of 2β = 15º, 30º, 60º, 75º, and 90º. The loading was performed by varying the loading angle formed by the longitudinal axis of the PMMA plate with respect to the loading direction, as shown in Fig. 4(b). The test loading angles were γ = 0º (Mode I), 30º, 45º, 60º, 75º and 90º (Mode II). The specimen loading was carried out in an INSTRON-4481 servo-controlled testing machine. The tests were conducted in air at room temperature and the crosshead speed was 0.5mm/min.

The critical loads at fracture are tabulated in Table 1. Since some specimens ruptured at the fixing holes,

Table 1. Fracture load of V-notched PMMA specimens.

Loading angle(γ)	Notch angle(2β)	Fracture load [kN]				
		15°	30°	60°	75°	90°
0°		0.341	0.379	0.399	0.422	0.409
0°		0.333	0.366	0.382	0.374	0.408
0°		0.344	0.378	0.39	0.419	0.42
30°		0.609	0.662	0.675	0.698	0.713
30°		0.578	0.557	0.649	0.657	0.748
30°		0.627	0.748	0.674	0.734	0.661
45°		0.557	0.598	0.53	0.766	0.961
45°		0.565	0.716	0.625	0.694	0.981
45°		0.532	0.602	0.57	0.746	-
60°		0.492	0.574	0.894	0.807	1.047
60°		0.534	0.553	0.598	0.79	1.049
60°		0.474	0.483	0.769	0.927	-
75°		0.575	0.719	1.13	1.012	2.024
75°		0.596	0.715	1.464	1.681	1.952
75°		0.684	0.833	0.824	1.488	-
90°		0.722	0.501	1.37	1.853	2.25
90°		0.882	0.722	1.552	1.93	-
90°		0.667	0.882	-	1.906	-

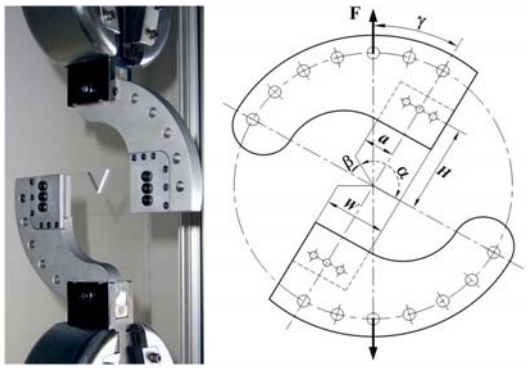

(a) (b)

Fig. 4. Photograph and configuration of the loading fixture with a V-notch specimen.

several fracture loads were not recorded in Table 1. The experimental data in this research were similar in trend to those of Seweryn et al. [12]. As shown in Table 1, the fracture load increases with the notch angle and loading angle. Furthermore, the fracture loads in Mode II for γ = 90° are remarkably larger than those under Mode I for γ = 0°. The critical values for γ = 30° suddenly increase in comparison with those for γ = 0° and are produced the analogous value in all the notch angles. The measured value of θ_o for the broken specimens is presented in

Table 2. θ_o measured for the broken V-notched PMMA plates.

Loading angle(γ)	Notch angle(2β)	Crack orientation				
		15°	30°	60°	75°	90°
0°		0°	1.5°	0.5°	1°	1°
0°		1°	1°	1.5°	1°	1°
0°		1°	0°	0.5°	1°	0°
30°		36°	36.5°	33.5°	30°	30°
30°		40°	36.5°	32°	31.5°	27°
30°		38.5°	40°	32°	29°	28°
45°		49°	47.5°	35°	40.5°	42°
45°		50°	54°	44°	40°	41.5°
45°		50°	48.5°	39.5°	42°	-
60°		53°	53.5°	49.5°	45.5°	43.5°
60°		57°	52.5°	47°	45.5°	44.5°
60°		57°	54°	50°	46°	-
75°		62°	61°	62.5°	50°	58.5°
75°		65°	64.5°	58.5°	59°	59°
75°		56°	60°	61°	62°	-
90°		66°	58.5°	65°	59°	48°
90°		66.5°	66°	66°	63°	-
90°		68°	66.5°	-	62°	-

Table 2. It was observed that θ_o increases with the loading angle, whereas θ_o decreases as the notch angle increases. σ_c was also obtained by using the test results of seven tensile specimens. The test results give σ_c = 61.7MPa with a standard deviation of 5.1 MPa. All the tensile fractures occurred at the maximum load without necking.

4.2 Determination of the stress intensity factors

To calculate the stress intensity factors of a V-notch, the RWCIM was used. K_I^n and K_{II}^n associated with A_{R1} and A_{I1}, respectively, can be calculated by using the RWCIM. The stresses and displacements required for the calculation are obtained by a finite element analysis, which uses the commercial finite element analysis code ANSYS [22].

For verifying the validity and accuracy of the RWCIM program in the mixed mode condition, the stresses σ_{rr} for the FEA and RWCIM on the contour of radius r =0.2 a with respect to the V-notch tip in Fig. 4(b) are compared. Three cases are examined. The first case is 2β =20°, a/W =0.5, H/W =1.5, and γ =45°; the second case is 2β =60 ° and γ =90°; and the third case is 2β =90° and γ =60°, as shown in Fig. 4(b). The FE model for the

Table 3. Eigenvector coefficient associated with each eigenvalue.

Case	Eigenvalue		Associated eigenvector coefficient	
1	ϕ_1	0.5004	$A_{R1}(\varphi_1)$	6.2706
	ϕ_2	1.1254	$A_{R2}(\varphi_2)$	-0.0461
	ϕ_3	1.4976	$A_{R3}(\varphi_3)$	-0.0940
	η_1	0.5620	$A_{I1}(\eta_1)$	2.8798
	η_2	1	$A_{I2}(\eta_2)$	1.5051
	η_3	1.6923	$A_{I3}(\eta_3)$	0.0290
	η_4	1.9914	$A_{I4}(\eta_4)$	0.0026
2	ϕ_1	0.5122	$A_{R1}(\varphi_1)$	0.0000
	η_1	0.7309	$A_{I1}(\eta_1)$	4.1242
	η_2	1	$A_{I2}(\eta_2)$	3.2438
3	ϕ_1	0.5445	$A_{R1}(\varphi_1)$	3.5451
	η_1	0.9085	$A_{I1}(\eta_1)$	6.6413
	η_2	1	$A_{I2}(\eta_2)$	-1.4914

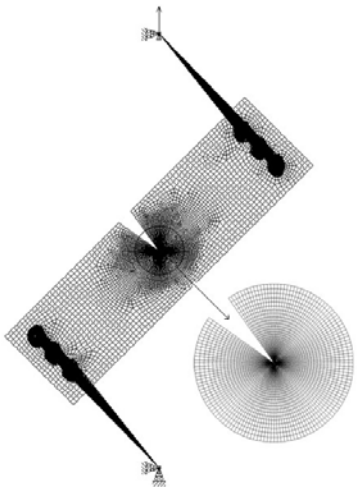

Fig. 5. FE-model for the first case with 2β =20º, a/W =0.5, H/W =1.5, and γ =45º.

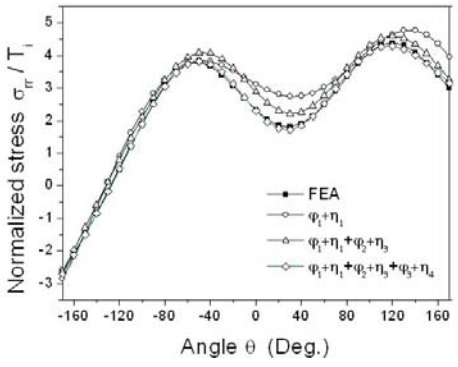

Fig. 6. Comparison of $(\sigma_{rr})_{FEA}$ and $(\sigma_{rr})_{RWCIM}$ according to the number of eigenvalues on the contour of radius r =0.2 a, when a/W =0.5, H/W =1.5, 2β =20º, and γ =45º.

first case is shown in Fig. 5. Loading point and fixed holes were connected via multipoint constraint equation (MPC) [22] to distribute the force applied at the loading point to nodes around the holes, taking into account the geometry of the fixed holes. The eigenvector coefficients were evaluated under the plane stress condition. Similar analyses have been carried out for all the other cases, and the results of those for each case are presented in Table 3. The second eigenvalue η_2 =1 of Mode II is an eigenvalue related to the rotational component of rigid body motion [19]. Therefore, the eigenvalue η_2 =1 cannot affect the stress distribution near the notch tip. In the first case, $(\sigma_{rr})_{FEA}$ obtained by using the finite element analysis and $(\sigma_{rr})_{RWCIM}$ calculated by substituting the eigenvector coefficients determined from the RWCIM program into the radial stress component σ_{rr} of Eq. (2) are shown in Fig. 6; these stresses are normalized by traction T_i $(=F/(t\times W))$ with respect to tensile loading. It is shown that there is a considerable difference in the values between $(\sigma_{rr})_{FEA}$ and $(\sigma_{rr})_{RWCIM}$ obtained by using only the terms of the singular eigenvalues φ_1 and η_1. By adding the terms of the nonsingular eigenvalues to σ_{rr} of Eq. (2), $(\sigma_{rr})_{RWCIM}$ approaches $(\sigma_{rr})_{FEA}$, as shown in Fig. 6. The second case is subjected to Mode II loading. Hence, the eigenvector coefficients associated with Mode I become zero, as shown in Table 3. Fig. 7 shows that $(\sigma_{rr})_{RWCIM}$ determined by the Mode II singular eigenvalue η_1 is consistent with $(\sigma_{rr})_{FEA}$. In the third case, Fig. 8 shows that the value of $(\sigma_{rr})_{RWCIM}$ calculated by using only the singular terms is in good agreement with that of $(\sigma_{rr})_{FEA}$.

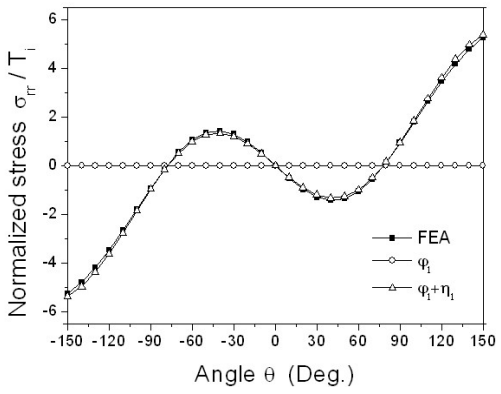

Fig. 7. Comparison of $(\sigma_{rr})_{FEA}$ and $(\sigma_{rr})_{RWCIM}$ according to the number of eigenvalues on the contour of radius r =0.2a, when a/W =0.5, H/W =1.5, 2β =60º, and γ =90º.

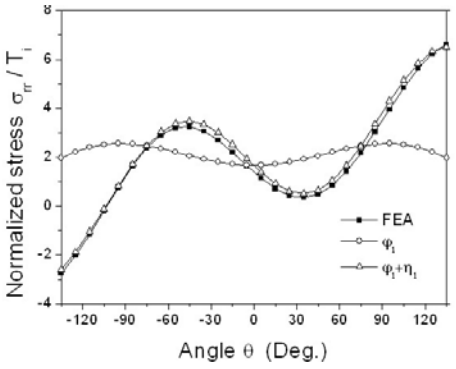

Fig. 8. Comparison of $(\sigma_{rr})_{FEA}$ and $(\sigma_{rr})_{RWCIM}$ according to the number of eigenvalues on the contour of radius r =0.2 a, when a/W =0.5, H/W =1.5, 2β =90º, and γ =60º.

4.3 Verification of the proposed fracture criterion

The critical loads at fracture were measured to calculate $A_{R1}(\varphi_1)$ and $A_{I1}(\eta_1)$ through numerical analysis by using the RWCIM program. The critical stress intensity factors were determined from the RWCIM program by considering the stresses and displacements computed from the finite element analysis using the critical loads at fracture. In the finite element analysis, the plane stress condition was used and the elastic properties of the PMMA material are Young's modulus $E = 3391$ MPa and Poisson's ratio ν =0.36.

To verify the proposed fracture criterion, the critical stress intensity factors determined by the fracture load will be compared with the fracture curve predicted by the criterion of Eqs. (14) and (15). The crack orientations measured for the broken specimens will also be compared with the results predicted by the criterion of Eq. (13).

The value of d_o should be determined in order to predict the crack initiation. However, it is difficult that PMMA specimens with the configuration of a crack are fabricated exactly. Therefore, instead of determining d_o from Eq. (12) by using K_C, it can be obtained by substituting the K_{Icr}^n for each V-notch angle of 2β = 15º, 30º, 60º, 75º, and 90º into Eq. (11) because d_o is a material constant. In this paper, the mean value of all the results obtained from the above substitution is used as the material constant d_o and the fracture toughness K_C can be also calculated from Eq. (12) by using the mean value d_o. These values are presented in Table 4. Fig. 9 shows K_{Icr}^n as predicted by Eq. (11) using the mean value d_o and the experimental results.

Table 4. d_o and K_c for PMMA.

Material property	Material constant d_o [m]	Fracture toughness K_c [MPa · $m^{0.5}$]
Value	0.0002863	1.3087

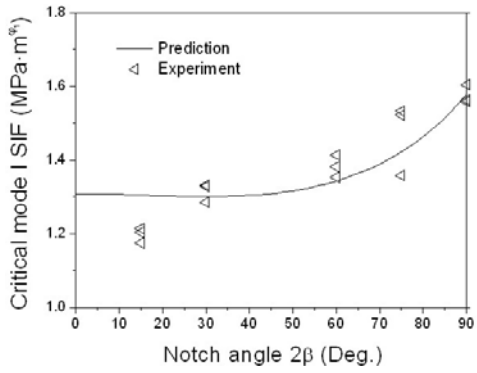

Fig. 9. K_{Icr}^n predicted by d_o under Mode I loading.

Figs. 10(b)-(f) show a comparison of the predicted curves of the critical stress intensity factors of Eqs. (14) and (15) for each V-notch angle of 2β =15º, 30º, 60º, 75º, and 90º with the experimental results in the mixed mode condition. Fig. 10(a) shows only the predicted curves of the critical stress intensity factors for 2β =0º without the experimental results. The crack orientations predicted by Eq. (13) are also shown with the experimental results in Figs. 11(b)-(f). Fig. 11(a) shows only the predicted crack orientations for 2β =0º without the experimental results. It is well known that θ_o becomes zero for all notch angles under Mode I loading. However, under Mode II loading, θ_o varies from θ_o =70.5288º in the case of 2β =0º to 53.7579º in the case of 2β =90º as shown in Fig. 12. The results show that all the fracture curves may provide a conservative estimate of the fracture strength. This fact is due to sharp V-notch machining difficulties. We know that the sharpness of the tip of a specimen is important. But, in V-notch machining, it is unavoidable that V-notches have the notch root radii. The small rounded shape of the notch tips will increase the fracture load of the specimens. Hence, it can be stated that the predicted and experimental results are in nearly good agreement.

We examined once more using the experimental data for 2β =20º, 40º, 60º, and 80º given by Seweryn et al. [12] for PMMA. The material properties of PMMA [23] are E =3300MPa and ν =0.35. The plane stress condition is used in the finite element

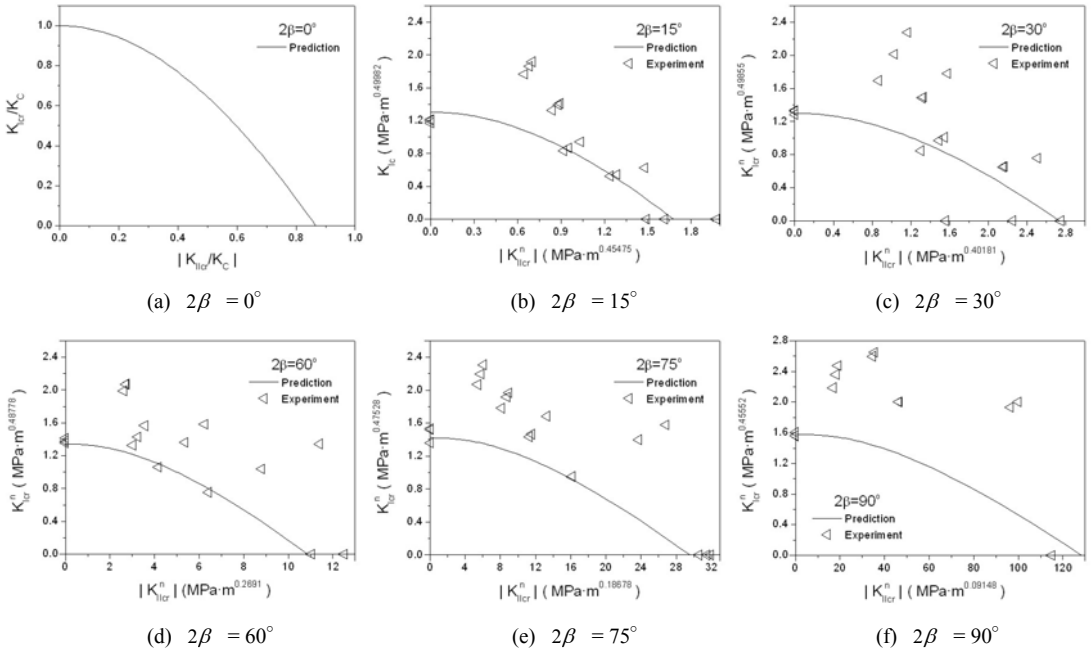

(a) $2\beta = 0^\circ$ (b) $2\beta = 15^\circ$ (c) $2\beta = 30^\circ$

(d) $2\beta = 60^\circ$ (e) $2\beta = 75^\circ$ (f) $2\beta = 90^\circ$

Fig. 10. Predicted fracture curves and experimental critical stress intensity factors under mixed mode loading.

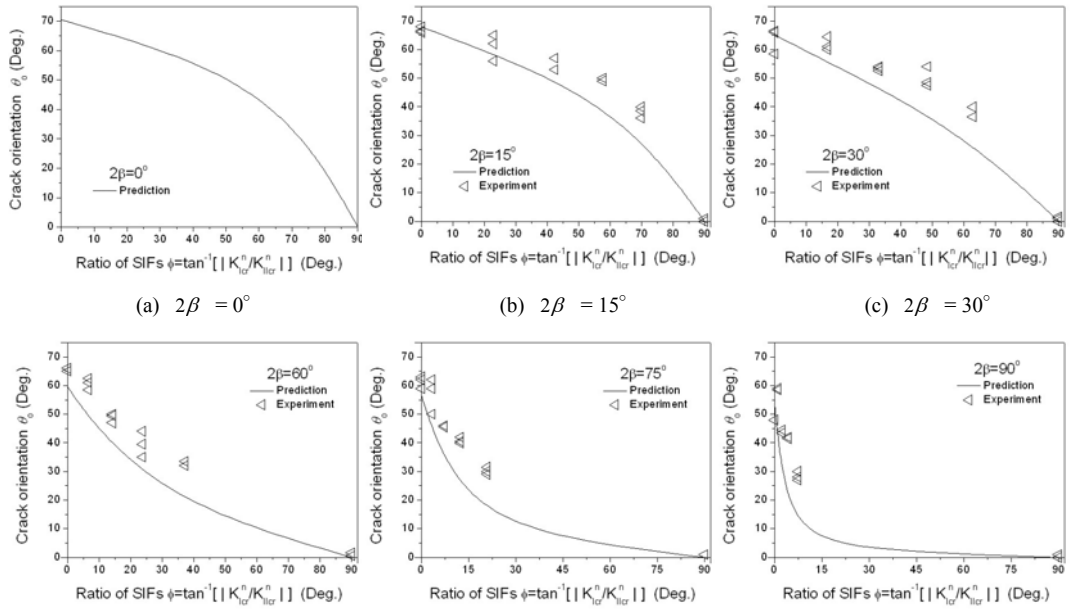

(a) $2\beta = 0^\circ$ (b) $2\beta = 15^\circ$ (c) $2\beta = 30^\circ$

(d) $2\beta = 60^\circ$ (e) $2\beta = 75^\circ$ (f) $2\beta = 90^\circ$

Fig. 11. Predicted and experimental crack orientation under mixed mode loading.

analysis. d_o was determined from Eq. (11) in the same manner. Its mean value was of $d_o = 0.0000872$ m and the value of K_C was 1.346MPa · m$^{0.5}$. Figs. 13(a)-(d) show the fracture curves as predicted by the criterion and the critical stress intensity factors obtained from the experiments. The value of θ_o predicted from Eq. (13) and the measured data of Seweryn et al. [12] are shown in Figs. 14(a)-(d).

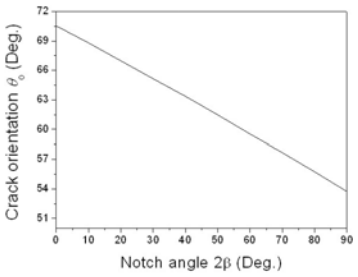

Fig. 12. Crack orientation for different notch angles under Mode II loading.

It can be stated that the predicted and experimental results are also in nearly good agreement.

5. Conclusions

The purpose of this paper is to propose a unified brittle fracture criterion for cracks and V-notches under mixed mode loading by extending the maximum circumferential stress criterion and Novozhilov's criterion.

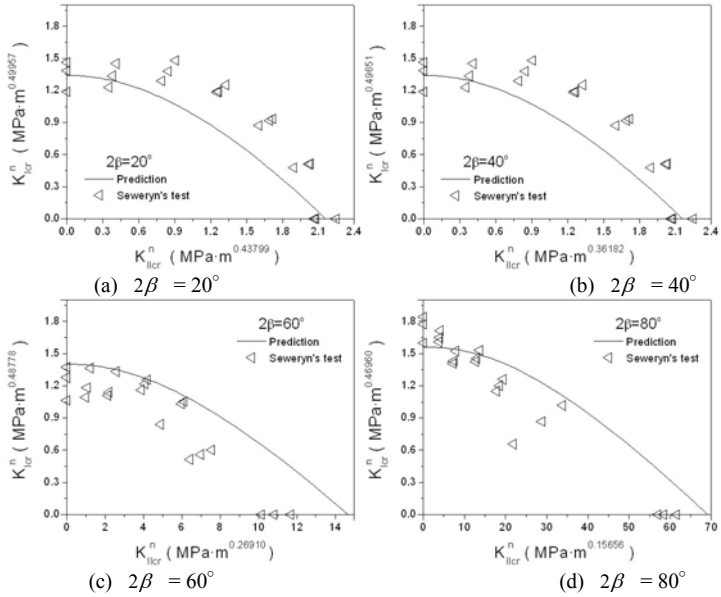

(a) $2\beta = 20^\circ$ (b) $2\beta = 40^\circ$

(c) $2\beta = 60^\circ$ (d) $2\beta = 80^\circ$

Fig. 13. Predicted fracture curves and Seweryn's experimental critical stress intensity factors under mixed mode loading.

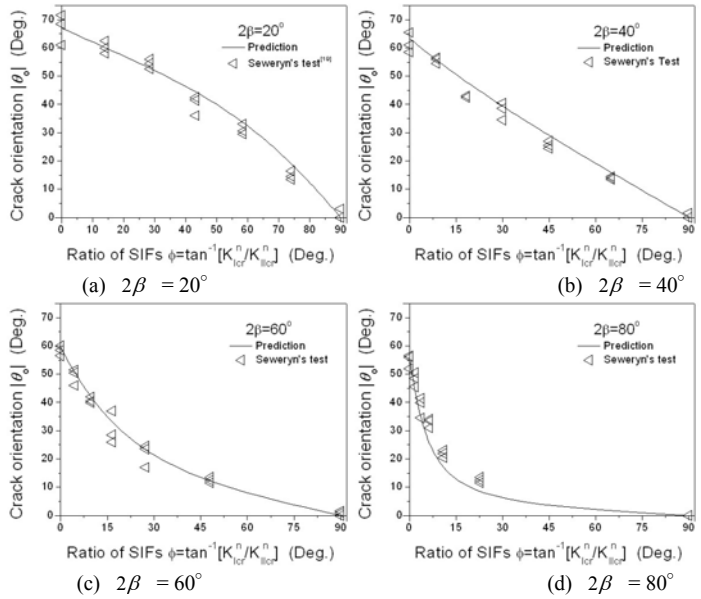

(a) $2\beta = 20^\circ$ (b) $2\beta = 40^\circ$

(c) $2\beta = 60^\circ$ (d) $2\beta = 80^\circ$

Fig. 14. Predicted and Seweryn's experimental crack orientation under mixed mode loading.

The crack initiations and orientations predicted by the proposed criterion agree nearly with our experimental results and Seweryn's tests.

This study shows that the proposed criterion is considerably simpler and can easily predict the crack initiation and orientation for cracks and V-notches under mixed mode loading.

Acknowledgment

This work was supported by the Kyungnam University Foundation Grant 2006.

References

[1] F. Erdogan and G. C. Sih, On the crack extension in plates under plane loading and transverse shear loading, *Journal of Basic Engineering, Transactions of ASME*, 85 (1963) 519-525.

[2] G. C. Sih, Strain energy density factor applied to mixed mode crack problems, *International Journal of Fracture*, 10 (1974) 305-321.

[3] M. A. Hussain, S. L. Pu and J. Underwood, Strain energy release rate for a crack under combined mode I and mode II, Fracture Analysis, ASTM STP 560, ASTM, Philadelphia, (1974) 2-28.

[4] A. Seweryn, Brittle fracture criterion for structures with sharp notches, *Engineering Fracture Mechanics*, 47 (1994) 673-681.

[5] V. V. Novozhilov, On necessary and sufficient criterion of brittle fracture, Prikladnaja Matematika, 33 (1969) 212-222.

[6] J. M. Whitney and R. J. Nuismer, Stress fracture criteria for laminated composites containing stress concentrations, *Journal of Composite Material*, 8 (1974) 253-265.

[7] M. L. Dunn and W. Suwito, Cunningham S. May CW. Fracture initiation at sharp notches mode I, mode II, and mild mixed mode loading, *International Journal of Fracture*, 84 (1997) 367-381.

[8] L. O. Jernkvist, Fracture of wood under mixed mode loading II. Experimental investigation of Picea abies, *Engineering Fracture Mechanics*, 68 (2001) 565-576

[9] M. Strandberg, Fracture at V-notches with contained plasticity, *Engineering Fracture Mechanics*, 69 (2002) 403-415.

[10] F. J. GÓmez and M. Elices, Fracture of components with V-shaped notches, *Engineering Fracture Mechanics*, 70 (2003) 1913-1927.

[11] F. J. GÓmez and M. Elices, A fracture criterion for blunted V-notched samples, *International Journal of Fracture*, 127 (2004) 239-264.

[12] A. Seweryn, S. Poskrobko and Z. MrÓz, Brittle fracture in plane elements with sharp notches under mixed-mode loading, *Journal of Engineering Mechanics*, 123 (1997) 535–543.

[13] J. L. Grenestedt, S. HallstrŐm and J. Kuttenkeuler, On cracks emanating from wedges in expanded PVC foam, *Engineering Fracture Mechanics*, 54 (1996) 445–456.

[14] S. HallstrŐm and J. L. Grenestedt, Mixed mode fracture of cracks and wedge shaped notches in expanded PVC form, *International Journal of Fracture*, 88 (1997) 343-358.

[15] M. Stern, E. B. Becker and R. S. Dunham, A contour integral computation of mixed-mode stress intensity factors, *International Journal of Fracture*, 12 (1976) 359–368.

[16] W. C. Carpenter, An improved technique for determining higher order eigenvector coefficients, *International Journal of Fracture*, 37 (1988) 107–121.

[17] W. C. Carpenter, Comments on the eigenvalue formulation of problems with cracks, V-notched cracks, and corners, *International Journal of Fracture*, 68 (1994) 75-87.

[18] W. C. Carpenter, Insensitivity of the reciprocal work contour integral method to higher order eigenvectors, *International Journal of Fracture*, 73 (1995) 93-108.

[19] J. K. Kim and S. B. Cho, An Analysis of Eigenvalues and Eigenvectors for V-notched Cracks in Pseudo-isotropic Dissimilar Materials, *International Journal of Precision Engineering and Manufacturing*, 3 (2002) 22-32.

[20] M. L. Williams, Stress singularities resulting from various boundary conditions in angular corners of plates in extension, *Journal of Applied Mechanics*, 19 (1952) 526–528.

[21] H. A. Richard, A new compact shear specimen, *International Journal of Fracture*, 17 (1981) R105-107

[22] ANSYS User's and Theory Manuals, Revision 10.0.

[23] A. Seweryn and A. Lukaszewicz, Verification of brittle fracture criteria for elements with V-shaped notches, *Engineering Fracture Mechanics*, 69 (2002) 1487-1510.